Influence of the crystalline electrical field on the magnetocaloric effect of $DyAl_2$, $ErAl_2$, and $DyNi_2$

P. J. von Ranke*
Ames Laboratory, Iowa State University, Ames, Iowa 50011-3020

V. K. Pecharsky† and K. A. Gschneidner, Jr.
Ames Laboratory, Iowa State University, Ames, Iowa 50011-3020
and Department of Materials Science and Engineering, Iowa State University, Ames, Iowa 50011-3020
(Received 17 March 1998)

Calculations of the magnetic entropy change ΔS_{mag} and the magnetocaloric effect (i.e., the adiabatic temperature change) ΔT_{ad} in $DyAl_2$, $ErAl_2$, and $DyNi_2$ using a Hamiltonian that takes into account the effects of crystalline electrical field and exchange interaction have been carried out. Good agreement between the theory and the experiment was obtained using the crystal-field parameters from inelastic neutron scattering for $DyAl_2$ and $ErAl_2$. The crystal-field parameters for $DyNi_2$, which were reported from magnetization measurements, did not give good agreement between the theory and the experiment. Using the experimental ΔS_{mag} versus T, and C_{mag} versus T (where C_{mag} is the magnetic heat capacity) we made an estimate of the crystal-field parameters for $DyNi_2$, which yield a satisfactory agreement between the theory and the experiment with regard to ΔS_{mag} and ΔT_{ad}. The appearance of a hump in the theoretical $\Delta S_{mag}(T)$ below the Curie temperature is discussed. [S0163-1829(98)05642-2]

I. INTRODUCTION

From a practical view point, the search for effective working substances for magnetic refrigeration remains important since further improvements in the overall magnetic refrigerator performance are critically dependent on the magnetocaloric properties of magnetic refrigerant materials. The interest in this research area was considerably increased since Brown[1] described a near-room-temperature magnetic refrigerator, which when compared with conventional gas compression/expansion engines has potential advantages in energy savings and elimination of harmful CFC's and HCFC's. Further improvements in energy efficiency require working substances with a large magnetocaloric effect, and the recent discovery[2] of the giant magnetocaloric effect in $Gd_5(Si_2Ge_2)$, give other impulses towards the development of magnetic cooling (and also heating) technology.[3]

From the theoretical viewpoint, the study of effective magnetic refrigerant materials is a fertile field, since it permits the application of a wide variety of physical models, which includes crystal lattice dynamics, band theory, and theory of magnetism, among others. The full understanding of the microscopic interactions, as well as the role of model parameters, is necessary for continued success in experimental investigations.

Our main goal in this work is to investigate the effect of crystalline electric fields (CEF's) on magnetocaloric properties of several well-known magnetic refrigerant materials. The two thermodynamic characteristics of the magnetocaloric effect are ΔS_{mag} (the isothermal magnetic entropy change) and ΔT_{ad} (the adiabatic temperature change), which are observed upon changes in the external magnetic field. These two quantities have fundamental importance for characterizing the potential of different materials for use in magnetic refrigerators; usually the larger the magnetocaloric effect the better. A general analysis of magnetic refrigeration and its optimization using the ΔS_{mag} and ΔT_{ad} together was combined in the concept of the refrigerant capacity by Wood and Potter.[4]

When the CEF interaction can be neglected, the quantitative theoretical analysis of the magnetocaloric effect in lanthanide materials is usually done by taking into account (1) the magnetic exchange interaction between magnetic ions in the molecular field approximation, (2) the lattice heat capacity in the Debye lattice approximation, and (3) the electronic heat capacity in the free-electron approximation.[5] However, in addition to the exchange interaction, CEF effects have a fundamental importance on the magnetic properties of the lanthanide ions in many of the intermetallic compounds. The CEF is created by the neighbors' charges surrounding the magnetic ion, and the simplest approach for accounting of the CEF is that of the so-called point-charge model.[6] When the lanthanide ion is introduced in a crystal lattice, the degeneracy of its total angular momentum is completely or partially removed due to CEF, yielding a set of magnetic energy levels, which in general depend on the direction of the exchange field.

In this paper we present the results of calculating the magnetocaloric effect (MCE) in three intermetallic compounds, $DyAl_2$, $ErAl_2$, and $DyNi_2$, and comparing it with the experimentally determined MCE. The MCE was theoretically calculated taking into account the exchange interaction in the molecular field approximation, the lattice and electronic entropies, and crystalline electric-field effects.

II. THEORY

All three compounds $DyAl_2$, $ErAl_2$, and $DyNi_2$ studied in this paper have cubic symmetry, and therefore CEF interactions can be described using two CEF parameters. Hence, in

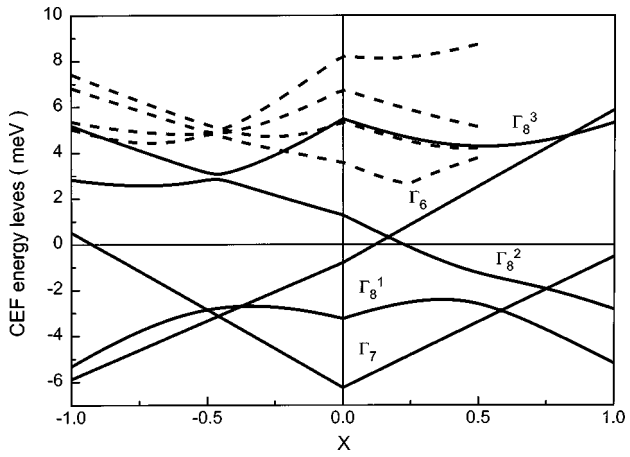

FIG. 1. The CEF energy levels vs the X CEF parameter for Dy and Er in cubic symmetry (solid lines). The dotted lines show the splitting of the Γ_8^3 ground state in the presence of the exchange interaction.

these lanthanide magnetic systems the two terms in the Hamiltonian, which describe their magnetic behavior in a crystal, are given by

$$\hat{H}=\hat{H}_{\mathrm{CEF}}+\hat{H}_{\mathrm{MAC}}, \tag{1}$$

where

$$\hat{H}_{\mathrm{CEF}}=W\left[\frac{X}{F_4}\,(O_4^0+5O_4^4)+\frac{(1-|X|)}{F_6}\,(O_6^0-21O_6^4)\right] \tag{2}$$

and

$$\hat{H}_{\mathrm{MAG}}=-g\mu_B H J^z. \tag{3}$$

Relation (2) is the single-ion CEF Hamiltonian written in the Lea, Leask, and Wolf (LLW) notation,[7] where W gives the CEF energy scale and X ($-1<X<1$) gives the relative contributions of the fourth and sixth degree in O_n^m Stevens' equivalent operators.[8] The constants F_4 and F_6 have the values $F_4=60$ and $F_6=13\,862$. In presence of a cubic CEF both Dy and Er have the following set of CEF levels: Γ_8^3 (quadruplet), Γ_8^2 (quadruplet), Γ_8^1 (quadruplet), Γ_7 (doublet), and Γ_6 (doublet). The solid lines in Fig. 1 represent the energy position of these levels as functions of the X CEF parameter corresponding to $W=-0.019$ meV. It is interesting to note that for $W<0$ and $-1<X\leqslant 0.84$, the ground state is Γ_8^3.

Relation (3) is the single-ion magnetic Hamiltonian, taken in the molecular field approximation, where g is the Lande factor, μ_B is the Bohr magneton, and $H=H_0+\lambda g\mu_B\langle J^z\rangle$ is the external magnetic field plus the effective molecular field with the molecular-field constant λ, and $\langle J^z\rangle$ being the average value of the total angular momentum in the easy magnetic direction. For $DyAl_2$, $ErAl_2$, and $DyNi_2$ the easy magnetic directions are the $\langle 100\rangle$,[9] $\langle 111\rangle$,[10] and $\langle 100\rangle$,[11] respectively.

The total entropy S_T of all three magnetic systems has three parts: (1) the magnetic entropy S_M, which includes the combined CEF and magnetic Hamiltonians; (2) the lattice entropy, S_{lat}, which accounts for lattice vibrations that will be treated in the Debye approximation; and (3) the electronic part S_{el}, which will be treated in the free-electron gas approximation. Hence,

$$S_T(H,T)=S_M(H,T)+S_{\mathrm{lat}}(T)+S_{\mathrm{el}}(T). \tag{4}$$

Since the lattice and electronic parts of total entropy do not depend on the magnetic field, the change of the total entropy ΔS_T with the magnetic field changing from H_1 to H_2 is $\Delta S_M=\Delta S_{\mathrm{mag}}$, and can be calculated from the Maxwell relation:

$$\Delta S_M(\Delta H,T)=S(H_2,T)-S(H_1,T)=\int_{H_1}^{H_2}\left(\frac{\partial M}{\partial T}\right)_H dH. \tag{5}$$

The magnetization M can be obtained from the self-consistent solution of the magnetic state equation,

$$M=g\mu_B\,\frac{\Sigma\langle\varepsilon_i|J^z|\varepsilon_i\rangle\exp[-(\varepsilon_i/KT)]}{\Sigma\,\exp[-(\varepsilon_i/KT)]}, \tag{6}$$

where ε_i and $|\varepsilon_i\rangle$ are, respectively, the energy eigenvalues and eigenvectors of Hamiltonian (1).

The lattice entropy in the Debye approximation and the electronic entropy in the free-electron approximation are given by

$$S_{\mathrm{lat}}=-3R\,\ln[1-\exp(\Theta_D/T)]+12R\left(\frac{T}{\Theta_D}\right)^3\int_0^{\Theta_D/T}\frac{x^3\,dx}{\exp(x)-1}, \tag{7}$$

and

$$S_{\mathrm{el}}=\gamma T, \tag{8}$$

where R is the universal gas constant, Θ_D is the Debye temperature, and γ is the electronic heat capacity coefficient. The adiabatic temperature change, ΔT_{ad}, for a magnetic field change from H_1 to H_2 can be calculated as the isentropic difference between the total entropy functions $S_T(H_2,T)$ and $S_T(H_1,T)$, which include all three contributions to the total entropy [Eq. (4)].

III. EXPERIMENT

The theoretically predicted magnetocaloric effect was compared with that obtained from experimental data. Both ΔS_{mag} and ΔT_{ad} were calculated from the experimentally measured heat capacity as a function of temperature in magnetic fields 0, 2, and 5 T. The details concerning the calorimeter and the heat capacity measurement procedures can be found in Ref. 12, and the details of processing the heat capacity data to yield ΔS_{mag} and ΔT_{ad} are given in Ref. 13. The detailed results concerning the magnetic heat capacity of $DyAl_2$, $ErAl_2$, and $DyNi_2$ will be published elsewhere.

IV. RESULTS FOR $DyAl_2$, $ErAl_2$, AND $DyNi_2$

In order to theoretically calculate the temperature dependence of magnetic entropy change ΔS_{mag} and the adiabatic temperature change ΔT_{ad} in $DyAl_2$, $ErAl_2$, and $DyNi_2$ for two magnetic field changes ($0\rightarrow 2$ T) and ($0\rightarrow 5$ T), we have carried out the following numerical calculations. Since

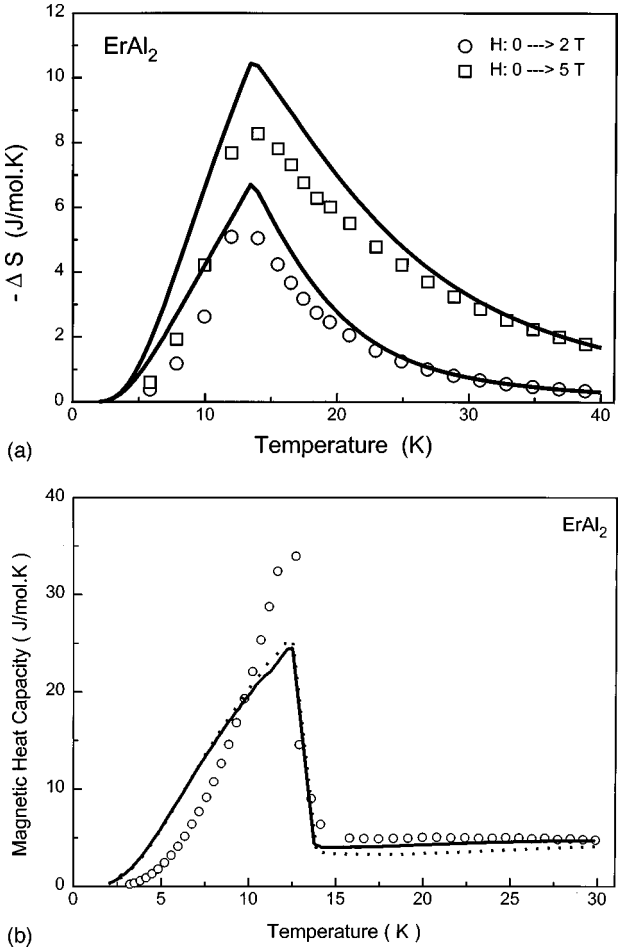

FIG. 2. (a) Temperature dependence of ΔS_{mag} in $ErAl_2$ for a magnetic-field change from 0 to 2 T and 0 to 5 T. The solid lines represent the theoretical results obtained using $X=-0.262$, $W=-0.0252$ meV from Ref. 15 and $\lambda=13.5(T^2/\mathrm{meV})$. The open circles and squares show the experimental data (Ref. 14). (b) Magnetic heat capacity in zero magnetic field vs temperature in $ErAl_2$. Open circles show the experimental data (Ref. 14) and the solid line represents the theoretical results obtained using $X=-0.262$, $W=-0.0252$ meV from Ref. 15 and $\lambda=13.5(T^2/\mathrm{meV})$. The dotted theoretical line was obtained using $(W,X,\lambda)=(-0.03\ \mathrm{meV},\ -0.3,\ 13.5T^2/\mathrm{meV})$.

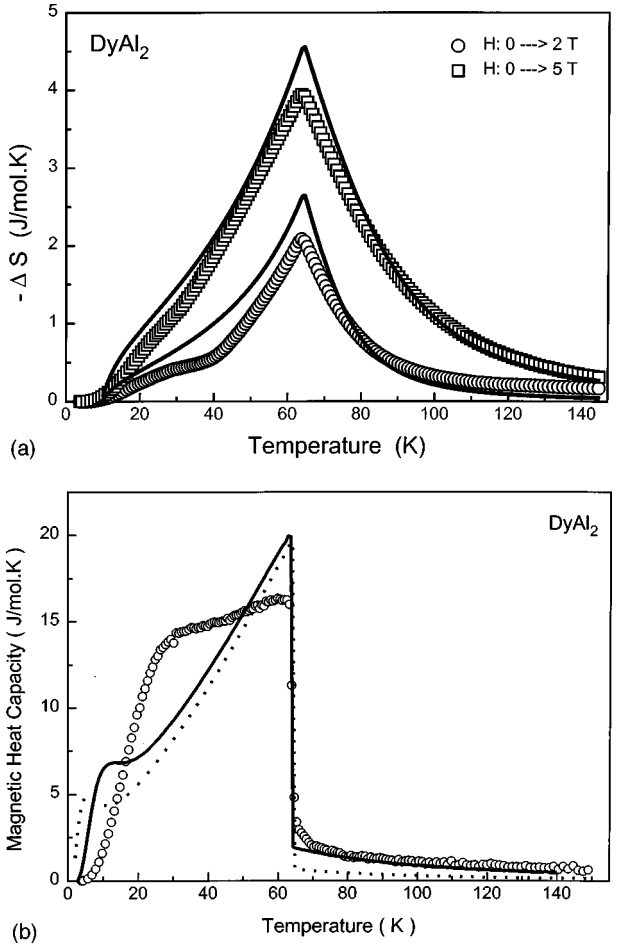

FIG. 3. (a) Temperature dependence of ΔS_{mag} in $DyAl_2$ for a magnetic-field change from 0 to 2 T and 0 to 5 T. The solid lines represent the theoretical results obtained using $X=0.3$, $W=0.011$ meV from Ref. 15 and $\lambda=44.0(T^2/\mathrm{meV})$. The open circles and squares show the experimental data (Ref. 14). (b) Magnetic heat capacity in zero magnetic field vs temperature in $DyAl_2$. Open circles show the experimental data (Ref. 14) and the dotted line represents the theoretical results using $X=0.3$, $W=0.011$ meV from Ref. 15 and $\lambda=44.0(T^2/\mathrm{meV})$. The solid line represents the theoretical results using $(W,X,\lambda)=(0.0184\ \mathrm{meV},\ 0.21,\ 44.0T^2/\mathrm{meV})$.

both Er and Dy elements have the same total angular momentum $J=\frac{15}{2}$ we built a 16×16 square matrix using the CEF and magnetic Hamiltonian. Updating this matrix with the two CEF parameters X,W and the exchange parameter λ we obtain a set of energy eigenvalues and eigenvectors in self-consistent condition solving Eq. (6) simultaneously. This allows one to determine the temperature and magnetic-field dependence of the magnetization [Eq. (6)] and the magnetic entropy change [Eq. (5)].

Figure 2(a) shows the temperature dependence of the magnetic entropy change in $ErAl_2$ for a magnetic-field change from 0 to 2 and from 0 to 5 T. The open squares and circles represent experimental data.[14] The solid lines represent theoretical results obtained from our calculations using the CEF parameters determined from neutron scattering measurements[15] $X=-0.262$ and $W=-0.0252$ meV and the exchange parameter $\lambda=13.3(T^2/\mathrm{meV})$. The exchange parameter was adjusted from our theoretical calculation to yield the Curie temperature equal to the temperature of the experimental peak in ΔS_{mag}, which is associated with the ferromagnetic to paramagnetic phase transition. The experimental[14] and theoretical curves for zero-field magnetic heat capacity versus temperature in $ErAl_2$ are show in Fig. 2(b). The solid line represents the theoretical results obtained using the CEF parameters cited above. The dotted theoretical line was obtained using CEF parameters $X=-0.3$ and $W=-0.03$ meV, which were determined from a local minimum in parameter space using a least-squares-fit procedure of the theoretical magnetic heat capacity relative to the experimental magnetic heat capacity in zero field.

Figure 3(a) shows the temperature dependence of magnetic entropy change in $DyAl_2$ in the same magnetic fields as in Fig. 2. The solid line is calculated theoretically using the CEF parameters determined from neutron scattering measurements[15] $X=0.3$ and $W=0.011$ meV and the exchange parameter $\lambda=44.0(T^2/\mathrm{meV})$. Figure 3(b) shows the

experimental[14] and theoretical curves for magnetic heat capacity versus temperature in $DyAl_2$. Here the dotted line represents theoretical results obtained using the CEF parameters $X=0.3$ and $W=0.011$ meV, while the solid line represents the theoretical results using $X=0.21$ and $W=0.0184$ meV determined from the least-squares fit comparing the theoretical and experimental magnetic heat capacities in zero field. The relatively poor fit of the heat capacity data for $DyAl_2$ between ~20 and 50 K may be due to the spin reorientation transition from the ⟨100⟩ to the ⟨111⟩ (upon heating) at 40 K in $DyAl_2$.[16] No attempt was made to account for this transition in the theoretical calculations.

The results described above and depicted in Figs. 2(b) and 3(b) show that one can obtain reliable crystal-field parameters from the experimentally determined heat capacity after the electronic and lattice heat capacities have been subtracted off to give the magnetic heat capacity (also see below). Although this procedure does not give as precise values for CEF parameters as those obtained from neutron scattering measurements, in the absence of such measurements, a careful analysis of the heat capacity can lead to reliable CEF and exchange parameters; and, as will be shown below, they are probably more accurate than those obtained from magnetization measurements.

Figure 4(a) shows the experimental data[17] and theoretical results for the $DyNi_2$ magnetic entropy change and Fig. 4(b) for the magnetic heat capacity. The dotted lines were obtained using $X=0.49$ and $W=-0.0688$ meV (Ref. 11) from the magnetization measurements and $\lambda=17.5(T^2/\text{meV})$ determined from the procedure mentioned above. The agreement is poor, indicating that both CEF and exchange parameters used in the calculations were unrealistic. Because of this we used the procedure outlined above for $ErAl_2$ to find the best fit between experiment and theory for the zero-field magnetic heat capacity, and we found that the parameters $X=-0.1, W=-0.019$ meV, and $\lambda=15.5(T^2/\text{meV})$ yield a much better agreement, which is shown in Figs. 4(a) and 4(b) as solid lines. Note that the latter set of CEF and exchange parameters, leads to a hump below Curie temperature, which will be discussed below.

In order to calculate the adiabatic temperature change after having determined the magnetic entropy change produced by application of a magnetic field we need to include the lattice and electronic entropies given by Eqs. (7) and (8) and introduce two new parameters, namely, the Debye temperature Θ_D and the electronic heat capacity coefficient γ.

The lattice and electronic entropies of $DyAl_2$, $ErAl_2$, and $DyNi_2$ were determined assuming that both the Debye temperature and electronic heat capacity vary linearly in the RAl_2 and RNi_2 series of intermetallic compounds when the R component changes across the series from nonmagnetic La to nonmagnetic Lu. Therefore, for example in the case of $DyAl_2$, the total of lattice and electronic entropy would be a prorated sum of 35.7% (i.e., $\frac{5}{14}$) of the lattice and electronic entropy of $LaAl_2$ and 64.3% ($\frac{9}{14}$) of the lattice and electronic entropy of $LuAl_2$.

Using the experimental heat capacity data of $LaAl_2$,[18] $LuAl_2$,[19] $LaNi_{2.2}$ (Ref. 17) and $LuNi_2$ (Ref. 17) [note, that the compound $LaNi_2$ does not exist and, therefore, $LaNi_{2.2}$ may be considered as a good approximation of the former because of close relationship between the crystal structure of $LaNi_{2.2}$ (Ref. 20) and $LuNi_2$], we find that the electronic heat capacity coefficients are as follows: $LaAl_2$ ($\gamma=10.6$ mJ/mol K^2), $LuAl_2$ ($\gamma=5.5$ mJ/mol K^2), ''$LaNi_2$'' ($\gamma=4.8$ mJ/mol K^2), and $LuNi_2$ ($\gamma=4.6$ mJ/mol K^2). The estimated electronic contribution to the total entropy was calculated assuming that the electronic heat capacity coefficients are independent of temperature. The Debye temperature for the four nonmagnetic compounds were also determined from experimental heat capacities as functions of temperature, and these are shown in Fig. 5 with the close circles representing the calculated Θ_D and the solid lines representing the polynomial fits. The lattice entropies of $DyAl_2$, $ErAl_2$, and $DyNi_2$ were calculated using Eq. (7) and the prorated (as described

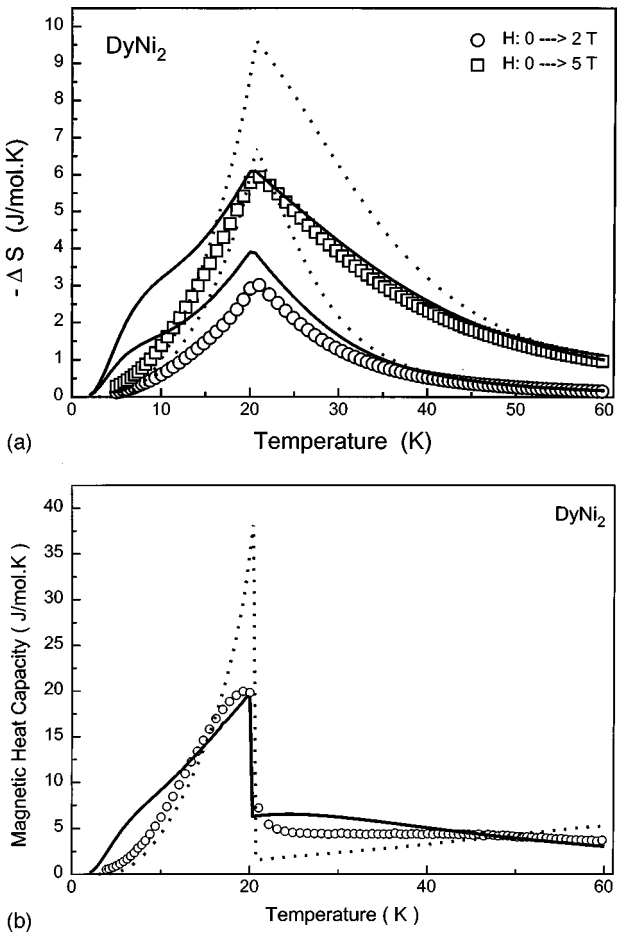

FIG. 4. (a) Temperature dependence of ΔS_{mag} in $DyNi_2$ for a magnetic-field change from 0 to 2 T and 0 to 5 T. The dotted lines represent the theoretical results using $X=0.49, W=-0.069$ meV, which were obtained from magnetization data (Ref. 11), and $\lambda=17.5(T^2/\text{meV})$. The solid lines represent the theoretical results using $X=-0.1, W=-0.019$ meV, and $\lambda=15.5(T^2/\text{meV})$, which were obtained from zero-field heat capacity data. The open circles and squares show the experimental data (Ref. 17). (b) Magnetic heat capacity in zero magnetic field vs temperature in $DyNi_2$. Open circles show the experimental data (Ref. 17) and the dotted line represents the theoretical results using $X=0.49, W=-0.069$ meV from magnetization data (Ref. 11) and $\lambda=17.5(T^2/\text{meV})$. The solid line represents the theoretical results using $(W,X,\lambda)=(-0.019\text{ meV}, -0.1, 15.5T^2/\text{meV})$, which were obtained from zero-field heat capacity data (Ref. 17).

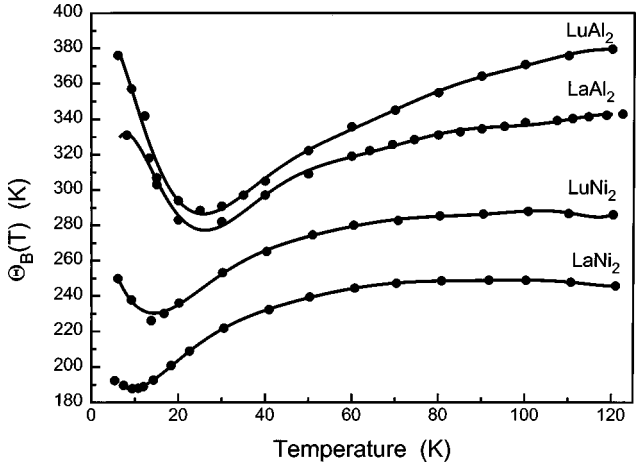

FIG. 5. The temperature dependencies of the Debye temperatures of $LaAl_2$, $LuAl_2$, $LaNi_2$, and $LuNi_2$. The solid circles show the effective Debye temperature and the solid lines are constructed using a ninth-degree polynomial regression fit.

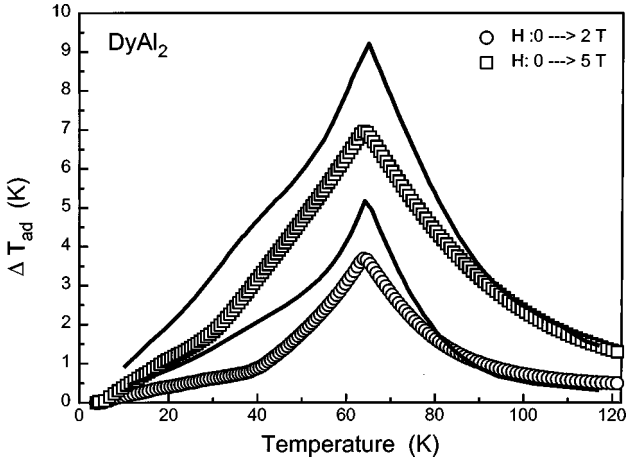

FIG. 7. The temperature dependence of ΔT_{ad} for $DyAl_2$ for a magnetic-field change from 0 to 2 T and 0 to 5 T. The solid lines represent the theoretical results and the open circles and squares show experimental data (Ref. 14).

above) Debye temperature of corresponding nonmagnetic counterparts.

Figures 6, 7, and 8 show the comparison of the experimentally determined and theoretically calculated ΔT_{ad} versus T for $ErAl_2$, $DyAl_2$, and $DyNi_2$, respectively. The crystal-field and exchange parameters considered here are the same as used in calculating ΔS_{mag} versus T.

V. DISCUSSION

As one can see from Figs. 2–4, and 6–8, using a Hamiltonian that combines the crystalline electrical-field effects and the magnetic exchange interactions, we were able to obtain good agreement between the experimental and theoretically calculated magnetocaloric effect in $ErAl_2$, $DyAl_2$, and $DyNi_2$. These results indicate that the simple molecular-field approximation permits a fairly accurate theoretical prediction of the magnetocaloric effect, at least in the case of cubic intermetallic compounds.

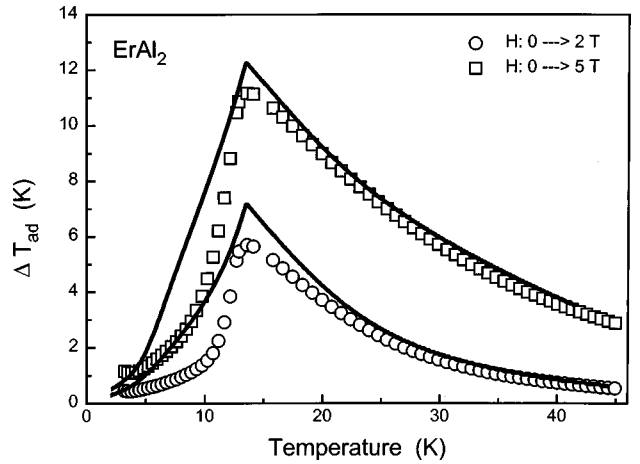

FIG. 6. The temperature dependence of ΔT_{ad} for $ErAl_2$ for a magnetic-field change from 0 to 2 T and 0 to 5 T. The solid lines represent the theoretical results and the open circles and squares show experimental data.

For both $ErAl_2$ and $DyAl_2$ satisfactory agreement was obtained when CEF parameters determined from inelastic neutron scattering experiments by Purwings and Leson[15] were used. In the case of $DyNi_2$, however, the CEF parameters were calculated by Gignoux and Givord[11] from magnetization measurements, and these yield a large discrepancy between the theory and the experiment [see Fig. 4(a) and Fig. 4(b), symbols and dotted lines]. Based on $\Delta S_{mag}(\Delta H,T)$ and $C_M(0,T)$ determined experimentally from our magnetization and heat capacity measurements, we were able to adjust the CEF and exchange parameters for $DyNi_2$ to yield a much better agreement of theory and experiment [see Fig. 4(a) and Fig. 4(b), symbols and solid lines]. The adjustment of the CEF and exchange parameters is a valid approach, because the experimental $\Delta S_{mag}(\Delta H,T)$ and $C_M(0,T)$ data reflect the changes only in the magnetic entropy since the lattice and electronic entropies are magnetic-field-independent thermo-

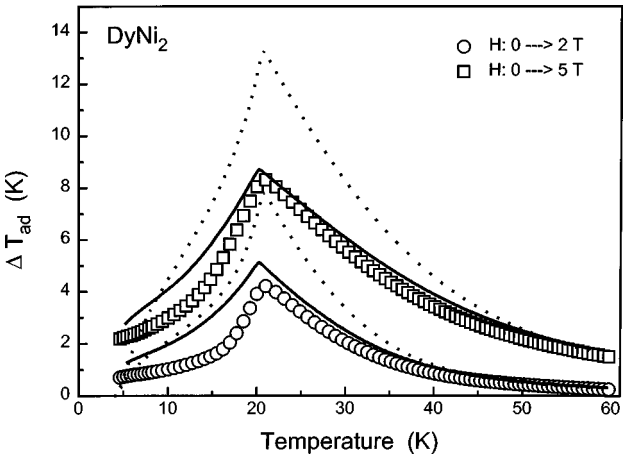

FIG. 8. The temperature dependence of ΔT_{ad} for $DyNi_2$ for magnetic-field change from 0 to 2 T and 0 to 5 T. The dotted and solid lines represent the theoretical results using $(W,X,\lambda)=(-0.069\ \text{meV},\ 0.49,\ 17.5T^2/\text{meV})$ and $(W,X,\lambda)=(-0.019\ \text{meV},\ -0.1,\ 15.5T^2/\text{meV})$, respectively. The open circles and squares show experimental data (Ref. 17).

dynamic functions. The adjusted CEF parameters for $DyNi_2$ are $X=-0.1$ and $W=-0.019$ meV, and they differ significantly from those reported earlier ($X=0.49$ and $W=-0.0688$ meV).[11]

It is worth noting, that in all cases ($ErAl_2$, $DyAl_2$, and $DyNi_2$) much better agreement between the magnetocaloric effect measured experimentally and that calculated from molecular field approximation is observed at temperatures exceeding the Curie temperature.

Figures 4(a) and 4(b) (solid lines) show that the theoretically predicted $\Delta S_{\rm mag}(\Delta H,T)$ develops a hump below the Curie temperature. These humps originate from the Γ_8^3 ground quadruplet CEF level. In the presence of the exchange interaction the degeneracy of the Γ_8^3 level is removed and this leads to the appearance of four separated singlet states. The dotted lines in Fig. 1 show the splitting of the Γ_8^3 ground state in the presence of the exchange field $\lambda M/\mu_B$ calculated at $T=7.0$ K in $DyNi_2$. One can see that the energy separation between these singlet states strongly depends on the X CEF parameter and it has a minimum at $X=-0.48$ with a narrow energy splitting of 0.32 meV. When X deviates from $X=-0.48$ the energy splitting increases reaching the values of 2.24 meV at $X=-1$ and 4.9 meV at $X=0.5$.

Therefore, the dominance of the Γ_8^3 density of states at $X=-0.1$ for $DyNi_2$ gives origin to the humps observed at low temperature in the theoretical curves in Fig. 4(a) and Fig. 4(b). The $\Delta S_{\rm mag}$ obtained using the CEF parameters from Ref. 11 (dotted lines in Fig. 4) do not show these peaks, since in this case $X=0.49$ (i.e., low density of Γ_8^3 states).

Substituting $W=0$ into a CEF Hamiltonian, removes the large low-temperature hump but brings about small humps in $\Delta S_{\rm mag}$ and in magnetic heat capacity versus T curves below the Curie temperature. The appearance of the small humps in magnetic heat capacity was first noted by Fishman and Liu[21] who showed that they are intrinsic for large total angular moments and always exist when $J\geqslant 5/2$ in the context of the simple Heisenberg magnet model. Since we are considering compounds containing Dy and Er, which have the same and large total angular momentum ($J=\frac{15}{2}$), these humps are expected to contribute to the imperfect agreement between the theoretical and experimental $\Delta S_{\rm mag}$ and $\Delta T_{\rm ad}$ as functions of temperature and magnetic field below the Curie temperature, and their effect should be negligible above it. This explains the observed excellent agreement of experiment and theory above the Curie temperature. Finally, we can see that generally the theoretical curves for both $\Delta S_{\rm mag}$ and $\Delta T_{\rm ad}$ always exceed experimental values in the vicinity of the Curie temperature. This result was also expected since the theoretical calculations were performed assuming single-crystal specimens with the magnetic field applied parallel to the easy magnetizing direction, and the experimental data were obtained on polycrystalline samples.

Using the CEF parameters for $DyNi_2$ determined in this paper we observe much better agreement with the experimental data above 15 K compared with the results obtained using CEF parameters from magnetization measurement. On the other hand, the appearance of a hump in $\Delta S_{\rm mag}$ versus T which is not present in the experimental data for $DyNi_2$ indicates that our CEF parameters are also not the final determination of the CEF levels but shows that more refined experiments, such as inelastic neutron scattering, are needed to determine reliable values.

A full understanding of the origin of the hump [appearing below the Curie temperature on theoretical $\Delta S_{\rm mag}(\Delta H,T)$] associated with the density of CEF ground states in the presence of the exchange field, may have an impact on experimental investigations in order to design new materials with large magnetocaloric effects. When we theoretically consider the X CEF parameters near and at $X=-0.48$ (i.e., high density of Γ_8^3 states region) the hump transforms to a small peak at low temperature. Indeed such a peak has been observed experimentally in $(Dy_{1-x}Er_x)Al_2$ alloys with $x=0.5$,[16] where the Curie temperature has been shifted to ~40 K, i.e., the T_c is sufficiently high compared to the temperature of the small peak. This will be discussed in a future paper.

VI. CONCLUSION

As a result of this study we were able to show that the magnetocaloric behavior in terms of both the magnetic entropy change ($\Delta S_{\rm mag}$) and adiabatic temperature change ($\Delta T_{\rm ad}$) can be calculated theoretically from molecular-field theory in the presence of a cubic crystalline electric field. A comparison of the theoretically calculated magnetocaloric effect with that determined experimentally in $ErAl_2$, $DyAl_2$, and $DyNi_2$ shows good agreement. In the case of $ErAl_2$ and $DyAl_2$ satisfactory agreement between the theory and the experiment was obtained using the CEF parameters determined from inelastic neutron scattering experiments. For $DyNi_2$ the CEF parameters were adjusted using the experimental zero-magnetic-field heat capacity data.

The agreement between theory and experiment is better in the paramagnetic region (i.e., above the Curie temperature) than in the ordered state. Excessive magnetocaloric effect predicted by theory below the Curie temperature is most likely associated with the simplifications intrinsic to Heisenberg model and with the large angular momentum of Dy and Er and also with the fact that theoretical calculations were performed for single crystalline specimens with magnetic field parallel to their easy axes, while experimental data were obtained as polycrystalline samples.

The appearance of the large humps in the theoretical $\Delta S_{\rm mag}(\Delta H,T)$ behavior at the temperatures significantly below the Curie temperature in $DyNi_2$ is associated with the removable degeneracy of the Γ_8^3 crystalline electrical-field level and the density of states being the function of CEF parameters. The predicted humps exist because of the high density of states.

ACKNOWLEDGMENTS

The Ames Laboratory is operated by Iowa State University for the U.S. Department of Energy under Contract No. W-7405-ENG-82. This study was supported by the Office of Basic Energy Sciences, Materials Sciences Division. One of us (P. J. von Ranke) acknowledges the financial support of CNPq [Conselho Nacional de Desenvolvimento Cientifico e Tecnologico (Brasil)].

*Permanent address: Universidade do Estado do Rio de Janeiro, IF, Rua Sao Francisco Xavier, Rio de Janeiro-20550-013, Brasil.
†Author to whom correspondence should be sent: V. K. Pecharsky, 242A Spedding, Ames Laboratory, Iowa State University, Ames, Iowa, 50011-3020. E-mail: vitkp@ameslab.gov

[1] G. V. Brown, J. Appl. Phys. **47**, 3673 (1976).
[2] V. K. Pecharsky and K. A. Gschneidner, Jr., Phys. Rev. Lett. **78**, 4494 (1997).
[3] K. A. Gschneidner, Jr and V. K. Pecharsky, *Rare Earths: Science, Technology and Application III*, edited by R. C. Bautista, C. O. Bounds, T. W. Ellis, and B. T. Kilbourn (The Minerals, Metals & Materials Society, Warendale, PA, 1997).
[4] M. E. Wood, and W. H. Potter, Cryogenics **25**, 667 (1985).
[5] A. M. Tishin, Cryogenics **30**, 127 (1990).
[6] M. T. Hutchings, Solid State Phys. **16**, 227 (1964).
[7] K. R. Lea, M. J. M. Leask, and W. P. Wolf, J. Phys. Chem. Solids **33**, 1381 (1962).
[8] K. W. H. Stevens, Proc. Phys. Soc. London, Sect. A **65**, 209 (1952).
[9] N. Kaplan, E. Dormann, K. H. J. Buschow, and D. Lebenbaum, Phys. Rev. B **7**, 40 (1973).
[10] H. G. Purwins, Z. Phys. **233**, 27 (1970).
[11] D. Gignoux and F. Givord, Solid State Commun. **21**, 499 (1977).
[12] V. K. Pecharsky, J. O. Moorman, and K. A. Gschneidner, Jr., Rev. Sci. Instrum. **68**, 4196 (1997).
[13] V. K. Pecharsky and K. A. Gschneidner, Jr., Adv. Cryog. Eng. **42A**, 423 (1996).
[14] K. A. Gschneidner, Jr. and V. K. Pecharsky (unpublished).
[15] H. G. Purwins and A. Leson, Adv. Phys. **39**, 309 (1990).
[16] K. A. Gschneidner, Jr., V. K. Pecharsky, and S. K. Malik, Adv. Cryog. Eng. **42**, 475 (1996).
[17] Tiezhong Ma, K. A. Gschneidner, Jr., and V. K. Pecharsky (unpublished).
[18] C. Deenadas, A. W. Thompson, R. S. Graig, and W. E. Wallace, J. Phys. Chem. Solids **32**, 1843 (1971).
[19] T. Inoue, S. G. Sankar, R. S. Graig, W. E. Wallace, and K. A. Gschneidner, Jr., J. Phys. Chem. Solids **38**, 487 (1997).
[20] A. V. Klimyenko, J. Seuntjens, L. L. Miller, B. J. Beaudry, R. A. Jacobson, and K. A. Gschneidner, Jr., J. Less-Common Met. **144**, 133 (1998).
[21] R. S. Fishman and S. H. Liu, Phys. Rev. B **40**, 11 028 (1989).